J. Sens. Sens. Syst., 8, 57–66, 2019
https://doi.org/10.5194/jsss-8-57-2019

JSSS Journal of Sensors and Sensor Systems Open Access

A novel approach for road surface wetness detection with planar capacitive sensors

Jakob Döring, Lakshan Tharmakularajah, Jakob Happel, and Karl-Ludwig Krieger

Institute of Electrodynamics and Microelectronics (ITEM.ae), University of Bremen, Bremen, Germany

Correspondence: Jakob Döring (doering@item.uni-bremen.de)

Received: 17 August 2018 – Revised: 14 December 2018 – Accepted: 8 January 2019 – Published: 21 January 2019

Abstract. This paper presents a novel approach for detecting road surface wetness with planar capacitive sensors on the wheel arch liner of a motor vehicle. For this purpose, various design parameters of interdigital electrodes are studied by means of the finite element method (FEM). A suitable design for the detection of whirled-up water is proposed, which is manufactured on a flexible printed circuit board (PCB) and investigated in an experimental study. A test bench is built for that purpose, which includes a motor vehicle's front wheel arch liner and can simulate realistic road surface wetness conditions. Experimental results show the possibility of distinguishing between different road wetness conditions and confirm that a static wetting of the wheel arch liner can be detected. Finally, an application-specific sensor system is proposed, which is validated by experiments on a test bench and is integrated into a vehicle. Field test results show the feasibility of detecting different road wetness levels and demonstrate the potential of the presented approach.

1 Introduction

With the increasing level of automation in today's motor vehicles, the detection of road surface conditions becomes more important. Knowing the condition is of great relevance for highly or fully automated driving in demanding situations, caused by weather conditions, in order to return the motor vehicle from a critical situation to a safe state. Besides existing data from the environment and motor vehicle sensors, innovative approaches have to be investigated in order to reliably determine the road surface condition, since today's motor vehicles have no direct information about a road's current state. Therefore, both the safety of passengers and traffic participants can be increased. Road surface wetness is one of the conditions which has to be detected. A possible type of sensor suitable for the detection of road surface wetness is the capacitive sensor, due to its wide range of features.

Capacitive sensors have desirable features like robustness, low costs and flexibility in electrode design (Baxter, 1997; Brasseur, 2003; Hu and Yang, 2010). Therefore, they have been used in a wide range of applications. For instance they are used for proximity sensing (Chen and Luo, 1998), liquid level sensing in containers (Canbolat, 2009) or the detection of ice in liquid conveyor pipes (Happel et al., 2017). In the field of road surface condition detection there are still just a few publications about capacitive sensors. In Troiano et al. (2010) a low-cost capacitive sensor is presented which can be integrated into the roadway. The sensor can distinguish between dryness, moisture and ice but is for stationary use only. A mobile approach is proposed in Karuthedath and George (2012), where a capacitive sensor is attached to the bottom part of a remotely operated vehicle. It is supposed to detect the presence of ice on the surface of runways and roads.

In this work, we present a new approach for detecting road surface wetness with planar capacitive sensors on a motor vehicle's wheel arch liner. If the road surface is wet, the wheels of a motor vehicle cause water to whirl up. The capacitive sensor can detect water drops impinging upon the wheel arch liner and thus indirectly infer a wet road surface. Since a greater water film height leads to more water being whirled up and thus more drops impinging on the sensor, a basic distinction between different wetness levels is possible through an application-specific design of the sensor.

To show the feasibility of our approach, we investigate a suitably designed capacitive transducer in an experimental study at a test bench, including a motor vehicle's front

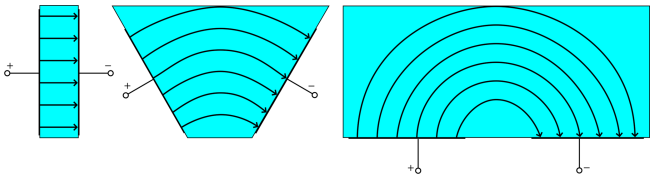

Figure 1. Gradual transition from a parallel plate capacitor to a planar capacitor, adapted from Mamishev et al. (2004).

wheel arch liner and a high-pressure pump with different water nozzles to simulate whirled-up water. Based on a video analysis, we define different realistic road condition scenarios and show the possibility of distinguishing between them. Furthermore, we propose a capacitive sensor system which is suitable for use in vehicles. By means of experiments with different wetness levels at a test bench, the sensor system is validated through a comparison to a reference measuring instrument. In a field test, the detection of road surface wetness with planar capacitive sensors is demonstrated by investigating different wetness levels and vehicle speeds on two test routes.

The remainder of this paper is organized as follows. In Sect. 2, the sensing principle of planar capacitive sensors with a focus on interdigital electrode design is described. Additionally, various parameters of such designs are investigated by means of the finite element method (FEM). Afterwards, the manufactured transducer is presented. Section 3 outlines the experimental setup and the laboratory tests. Subsequently, the experimental results are discussed. In Sect. 4, the sensor system is presented and integrated into a vehicle for a field test. Thereafter, the results are discussed. Finally, a conclusion is drawn in Sect. 5.

2 Planar capacitive sensors

In this section, we introduce planar capacitive sensors with a focus on interdigital electrode design. In addition, we demonstrate FEM simulation results for different electrode designs and propose a suitable one for the detection of whirled-up water. Finally, we present the manufactured capacitive transducer.

2.1 Sensing principle

The capacitive sensing principle is based on the interaction of a monitored medium and the electric field between the sensor electrodes (Hu and Yang, 2010). The applied electric field penetrates through the medium and generates electric displacement inside it. The charge stored between the sensor electrodes is altered by the electric displacement field, which leads to a changed capacitance of the transducer. This effect allows inferences about the permittivity of the monitored medium and thus the determination of system parameters that correlate with the permittivity of the medium (e.g., moisture).

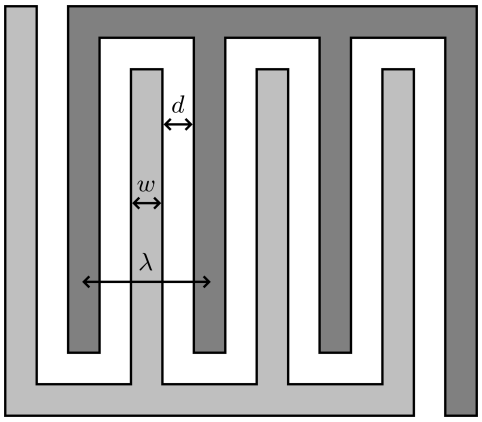

Figure 2. Schematic of an interdigital electrode structure. Both electrodes consist of four digits of width w separated by a distance d.

A commonly used capacitive sensor structure consists of two parallel plates, one representing the driving electrode and the other representing the sensing electrode (Hu and Yang, 2010). Between the parallel electrodes, an electric field is distributed. In this arrangement, the fringe field is negligible due to the much larger dimensions of the electrode surface compared to the electrode thickness. In case of a planar capacitive sensor, the electrodes are opened up, and the fringe field becomes predominant. Therefore, this kind of sensor is often denoted as a fringe field sensor in literature (Mamishev et al., 2004; Dean et al., 2012). Figure 1 shows the gradual transition from a parallel plate capacitor to a planar capacitor. It illustrates that the electric field lines penetrate into the monitored medium in all three cases. This shows the possibility of monitoring the medium from only one side with a planar capacitive transducer. There are advantages of dual-sided access, such as larger, more easily measurable capacitances and a more uniform distribution, but in some applications the advantage of single-sided access predominates.

Typically, interdigital electrode structures are used to design planar capacitive sensors, since the contribution of the fringing field effect in sensor capacitance is maximized (Mizuguchi et al., 2015). In this instance, the term interdigital describes a digit-like pattern of parallel in-plane electrodes (Mamishev et al., 2004). Both the sensing electrode and the driving electrode are built up by n digits of width w, separated by an insulating material of distance d, as shown in Fig. 2. Due to their periodicity, the correlation of width w and distance d is sometimes denoted as spatial wavelength λ in literature. It can be defined as the distance between the centerlines of adjacent digits belonging to the same electrode.

An important parameter for interdigital electrode structures is the penetration depth, which is approximately pro-

portional to λ (Li et al., 2004). In literature there is no unique definition, but one possible way to evaluate the penetration depth is to study how deep the electric field penetrates into a monitored medium (Da Silva, 2008). The point where 97 % of the asymptotic capacitance is reached is then defined as the penetration depth $\gamma_{97\,\%}$. By modifying the parameters n, w and d, it is possible to affect $\gamma_{97\,\%}$ and properties like measurement sensitivity, dynamic range and signal strength. Thus, an electrode design can be adjusted to its requirements.

2.2 Simulation

In contrast to classic electrode shapes, it is not trivial to analytically model planar capacitive sensors (Mamishev et al., 2004; Mizuguchi et al., 2015). Therefore, FEM is often used for sensor modeling, optimization and performance evaluation (Li et al., 2006). With regard to the experimental studies, presented in Sect. 3, different interdigital electrode designs are simulated in COMSOL Multiphysics. The goal of these simulations is to determine a suitable design for the detection of whirled-up water.

For the comparison of electrode designs with various values for the parameters n, w and d, three-dimensional electrostatic FEM simulations are executed. With regard to the manufacture of the transducer as a flexible printed circuit board (PCB), model parameters have been adjusted accordingly. For example the electrode area is 50 mm × 50 mm and has a back plane which serves as a shield. The relative permittivity ε_r is assumed to be equal to 1 for air, 80 for water and 3.4 for polyimide (PI), which serves as insulating material.

Since the process of water drops impinging upon the wheel arch liner and thereby upon the transducer is stochastic, we simplify the simulations by assuming a static water layer above the transducer. The water layer thickness referred in this section therefore refers to the water layer on the transducer surface and should not be confused with the thickness of the water film on the road surface. To assess different designs, the water layer thickness is varied from 0 to 10 mm. For the evaluation of $\gamma_{97\,\%}$, a water layer of 200 mm is additionally placed above the transducer to determine the asymptotic capacitance.

Due to the fixed transducer area and the restrictions at the later manufacture, we focus on four different electrode designs, which are presented in this section. Table 1 summarizes the design specifications and shows the evaluated penetration depths of the presented designs. There are two different values for both the ratio w/d and the number of digits n to reveal assets and drawbacks of these parameters. One effect can be observed for the penetration depth $\gamma_{97\,\%}$ in Table 1. In contrast to w/d, with increasing n from 4 to 7 and thereby decreasing spatial wavelength λ, $\gamma_{97\,\%}$ sinks by more than 59 %.

The simulated capacitance against water layer thickness curves are shown in Fig. 3. Increasing the number of digits results in a larger dynamic range and also in a higher measurement sensitivity, especially in close range. Comparing Design 1 and Design 2, there is an increase in the dynamic range of more than 48 %, whereas between Design 3 and Design 4, there is an increase of more than 63 %. Besides a higher absolute capacitance, which can be attributed to the electrode area, increasing w/d also effects the dynamic range. However, the percentage increase in the dynamic range is lower here, with around 24 % between Design 1 and Design 3 and more than 36 % between Design 2 and Design 4. Therefore, n has a bigger impact on the dynamic range than w/d.

The results reveal a trade-off between penetration depth and the dynamic range or measurement sensitivity. Since the capacitive transducer is placed on the inside of a wheel arch liner to detect whirled-up water, which impinges on it in the form of drops, a penetration depth of around 3.4 mm is sufficient and even advantageous compared to a penetration depth of 8.4 mm, considering that the electric field is concentrated on the relevant area. As Design 4 additionally has the highest dynamic range and measurement sensitivity, it is the most suitable of the simulated designs for the presented approach.

Table 1. Design specifications and evaluated penetration depth of the studied transducers.

	w	d	w/d	n	$\gamma_{97\,\%}$
Design 1	3.33 mm	3.33 mm	1	4	8.44 mm
Design 2	1.85 mm	1.85 mm	1	7	3.45 mm
Design 3	5.60 mm	0.70 mm	8	4	8.43 mm
Design 4	3.20 mm	0.40 mm	8	7	3.39 mm

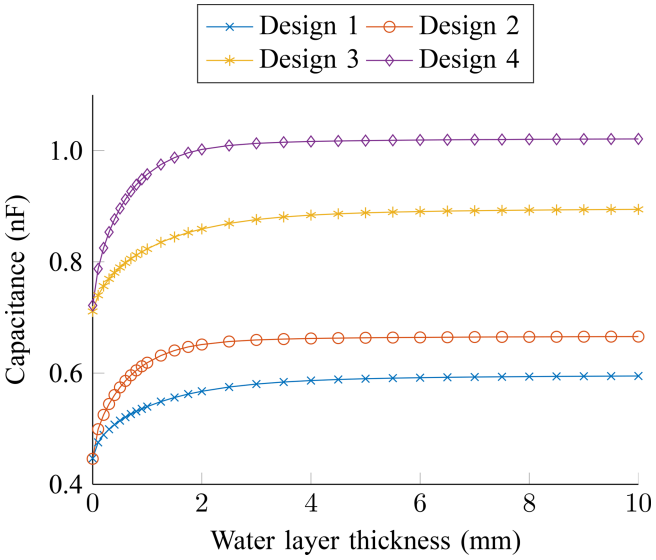

Figure 3. Simulated capacitance against water layer thickness for different electrode designs.

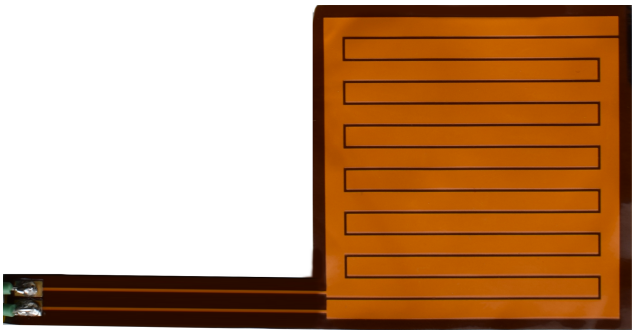

Figure 4. Planar capacitive transducer, manufactured as a flexible printed circuit board, with a thickness of 146 µm.

2.3 Manufacture

Planar capacitive transducers can be constructed in several ways, including manual construction, microelectromechanical systems (MEMS) and PCB technology (Hu and Yang, 2010). Due to the possibility of fabricating small-scale units with higher precision, the latter two are often preferred. Since PCB technology has further benefits, such as the possibility of fabricating larger transducers and lower per-unit costs, it is commonly used for the manufacturing (Dean et al., 2012; Mizuguchi et al., 2015).

For this work, the transducer is manufactured as a flexible PCB, which is ideally suited for the installation on the inside of a wheel arch liner. As a substrate for the symmetrical two-layer stack up of the PCB, PI is used which has a thickness of 50 µm. The interdigital electrode structure is realized as copper traces with a thickness 35 µm on the top layer and is protected by a 13 µm PI coverlay. On the bottom layer, which has the same dimensions, there is a guard plane used to shield the electrodes from noise. Considering all layers, the total thickness of the transducer adds up to 146 µm. The manufactured transducer, shown in Fig. 4, has a size of 54 mm × 54 mm, with an additional bracket for the feed lines of 9 mm × 54 mm.

3 Experimental study

In this section, the manufactured capacitive transducer is examined. Therefore, we first describe the experimental setup and the laboratory tests. Afterwards, we discuss the experimental results.

3.1 Setup

In order to investigate our approach of detecting whirled-up water on the inside of a motor vehicle's wheel arch liner, a test bench, shown in Fig. 5, is built. Aluminum profiles provide the scaffold for a front wheel arch liner made of polyethylene and a high-pressure pump with different water nozzles, used to simulate the whirled-up water. To realize different road surface condition scenarios, the pump's flow rate and the nozzle's angle can be adjusted from a PC. Therefore, a microcontroller is used which is connected to the PC via an RS-232 connection. Capacitance measurements are realized by an impedance analyzer (Keysight, E4990A-120) with an appropriate probe (42941A), connected to the planar capacitive transducer. The block diagram of the experimental setup for the measurements is shown in Fig. 6. Besides the described setup, there is a sensor system included which will be introduced in Sect. 4.1.

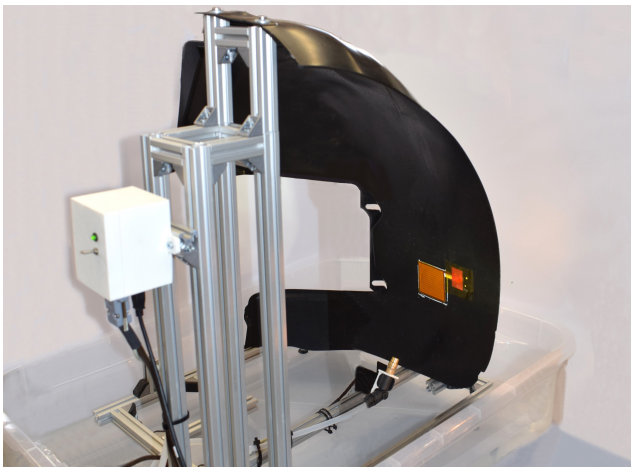

Figure 5. Test bench for the laboratory experiments, including a wheel arch liner, a high-pressure pump and a water nozzle.

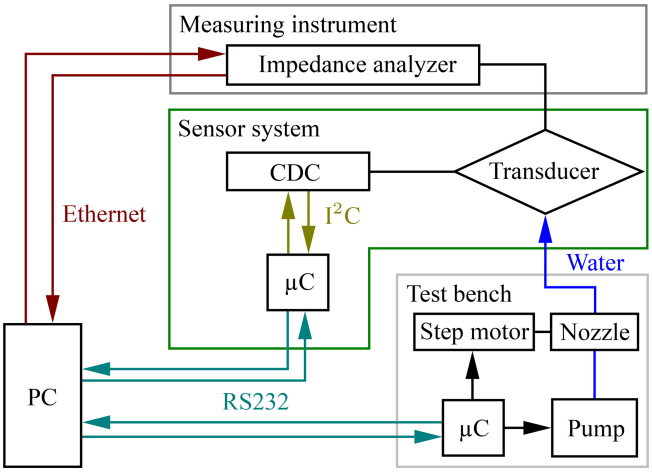

Figure 6. Block diagram of the experimental setup for measurements with a measuring instrument or a sensor system.

3.2 Experiments

The approach of detecting whirled-up water on a motor vehicle's wheel arch liner is investigated during laboratory tests. Therefore, the transducer, presented in Sect. 2.3, is placed on the inside of a wheel arch liner. The adequate position is

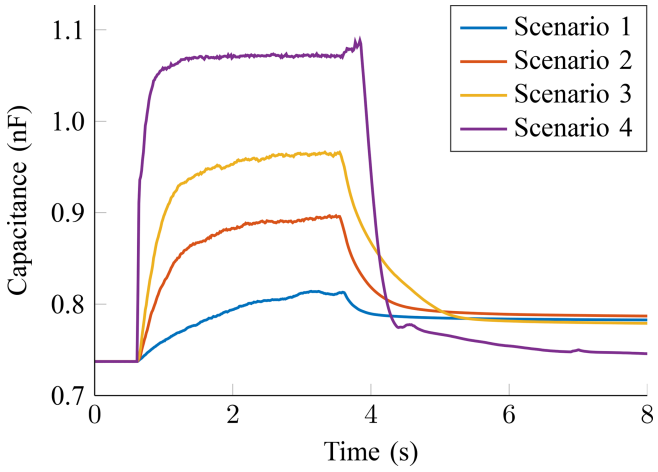

Figure 7. Experimental results of capacitance against time for realistic road surface scenarios.

chosen based on the analysis of a video recording of a wheel arch liner, captured during a test drive. The transducer's connections to an impedance analyzer are carried out through a small hole to the wheel arch liner's backside.

In addition to a suitable position for the transducer, we define four realistic and reproducible scenarios for the experiments based on the video analysis. Scenario 1 is realized by the finest and lowest quantity of water drops. Scenarios 2 and 3 are carried out with small drops, where the latter has a higher quantity of drops impinging on the investigated transducer. Scenario 4 provides the coarsest and highest quantity of drops. All scenarios are executed for 8 s, whereby the pump is active for approximately 3 s. Tap water at a temperature of 17 °C and an electrical conductivity of 365 µs cm^{-1} is used for the experiments. Each scenario is measured 10 times at an excitation frequency of 100 kHz.

3.3 Results

The experimental results of mean capacitance against time for the manufactured transducer are presented in Fig. 7, which shows the capacitance of every scenario and indicates varying rise times and differences in capacitance between the scenarios. Additionally, Table 2 summarizes the significant parameters of the figure. ΔC_1 corresponds to the difference in capacitance between the dry transducer and the end of water drops impinging on it, and ΔC_2 corresponds to the difference between the dry transducer and the measurement's end. The maximum standard deviation during the active pump is represented by $\sigma_{\max}$ and the time where 95 % of ΔC_1 values are reached by 3τ.

Since Scenario 1 is realized by the finest and lowest quantity of water drops, ΔC_1 has the smallest value, with 75 pF for this scenario. With the increasing size and quantity of drops, ΔC_1 increases to a maximum of 334 pF in Scenario 4. Since $\sigma_{\max}$ never exceeds 10.5 pF, it is possible to distinguish between the scenarios in all cases. The parameter 3τ may also be used to distinguish between road surface wetness conditions. While the capacitance in Scenario 1 needs 2.28 s to reach 95 % of the asymptotic value, in Scenario 4 the capacitance only needs 0.36 s.

Table 2. Experimental results for significant parameters of the manufactured transducer.

	ΔC_1	ΔC_2	$\sigma_{\max}$	3τ
Scenario 1	75.01 pF	45.48 pF	6.05 pF	2.28 s
Scenario 2	158.74 pF	49.77 pF	10.49 pF	1.59 s
Scenario 3	227.68 pF	41.79 pF	8.12 pF	1.43 s
Scenario 4	334.30 pF	8.60 pF	9.05 pF	0.36 s

After stopping the pump, Scenarios 1–3 show similar behaviors in capacitance by falling to a plateau higher than the one of the dry transducer, due to remaining drops. Since this offset, represented by ΔC_2, is assignable, the detection of a static wetting is possible. As the capacitance is higher for drops impinging upon the transducer in all scenarios, wetting is no drawback for the detection of new scenarios. Scenario 4 shows a different behavior when the pump is stopped. Due to the high quantity of drops impinging on the transducer and the area above, stopping the pump leads to a water film flowing above the transducer, which results in a capacitance peak. Thereby, in contrast to the other scenarios, the capacitance approximates faster to the value of a dry transducer. However, a static offset is still noticeable for the rest of the test.

4 Field test

In the first part of this section, we propose an application-specific sensor system which is validated in experiments. In the second part, we describe the vehicle integration of the sensor system and the setup for the field test. Finally, we discuss the field test results.

4.1 Validation of a sensor system

In order to investigate our approach in the field, a sensor system is needed for measurements in a vehicle, since an impedance analyzer is not convenient for this area of application. Besides the planar capacitive transducer presented in Sect. 2.3, the sensor system is realized by a microcontroller and a capacitance-to-digital converter (CDC), as shown in Fig. 6. In this work, the FDC2214 from Texas Instruments is used for the CDC component. The FDC2214 has a resolution of up to 28 bits, a maximum output rate of 4.08 ksps and a maximum input capacitance of 250 nF (Texas Instruments, 2015). In contrast to many other CDCs, FDC2214 uses an LC tank as a sensor. Therefore, a change in capacitance can be observed as a shift in resonant frequency. The device measures sensor frequency and outputs a digital value, which

is proportional to the ratio of sensor and the reference frequency that can be converted to an equivalent capacitance. For that reason, it is possible to adjust the excitation frequency from 10 kHz to 10 MHz by tuning the LC tank. In this work, the sensor system's excitation frequency is set to 100 kHz.

To validate the sensor system, the test bench presented in Sect. 3.1 is used. Hence, the experimental setup is expanded as shown in Fig. 6. The sensor system's microcontroller is connected to a PC via an RS232 connection and to the FDC2214 via an I^2C interface. For measurements the planar capacitive transducer is connected to FDC2214 through a small hole to the wheel arch liner's backside. For the validation of the sensor system, its results are compared to those obtained with the reference measuring instrument used in Sect. 3. For the comparison, a static capacitance offset by the FDC2214 is subtracted. Since the focus at this point is on the comparison between the sensor system and the measuring instrument, three arbitrary conditions (dry, wet and very wet) are defined instead of the scenarios described in Sect. 3.2 in order to minimize statistical deviations. For this reason, the wet and very wet conditions are realized by a steady active pump with different flow rates and nozzles. Thereby, various sizes and quantities of water drops impinge on the transducer. Each condition is measured 10 times for 10 s, with both the sensor system and the impedance analyzer at an excitation frequency of 100 kHz.

The experimental results for the comparison of the sensor system and the reference measuring instrument are presented in Fig. 8. It shows the mean capacitance of every condition, plotted consecutively, which indicates similar behavior for both the sensor system and the impedance analyzer for every condition. While the mean $\overline{x}$ of each condition is similar, there are differences in standard deviation σ, as summarized in Table 3. Besides variations among the condition due to stochastic effects of impinging water drops, there are differences between the sensor system and the impedance analyzer. Although in the dry condition σ is more than 94 % lower for the impedance analyzer, the sensor system's standard deviation with 0.59 pF is still low enough when considering the much higher differences in capacitance, even for small quantities of water drops impinging upon the transducer. While σ increases with wetness, the difference between the output of the sensor system and the impedance analyzer decreases. In the wet condition, the difference is about 49 %, and in the very wet condition, it is about 38 %. As already stated for the dry condition, even here, σ is low enough to reliably distinguish between different conditions. Therefore, our proposed sensor system is suitable for practical tests in a vehicle.

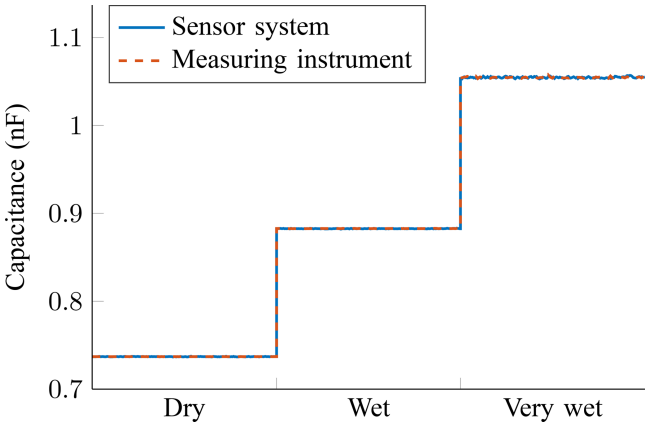

Figure 8. Experimental results of the capacitance against three different conditions for the comparison of the sensor system and the measuring instrument.

Table 3. Mean and standard deviation of the sensor system and the measuring instrument for three different conditions.

	Sensor system		Measuring instrument	
	$\overline{x}$	σ	$\overline{x}$	σ
Dry	737.70 pF	0.59 pF	737.70 pF	0.03 pF
Wet	882.70 pF	0.86 pF	882.71 pF	0.44 pF
Very wet	1054.65 pF	6.16 pF	1054.54 pF	3.84 pF

4.2 Vehicle integration and setup

In order to study our approach in a practical situation, the proposed sensor system is integrated into a test vehicle. For this purpose, a suitable enclosure is built from 3-D printing and can be mounted on the backside of a wheel arch liner. Figure 9 shows the integration of the sensor system into a test vehicle's front left wheel arch liner. For mounting the components, double-sided adhesive tape is used. While the transducer's adequate position is adopted from the test bench described in Sect. 3.2, the enclosure has to be mounted in a way to make the connections as short as possible between FDC2214 and the transducer to prevent high parasitic capacitances. Since there is sufficient room, the enclosure is mounted directly on the backside of the transducer's connections. Similar to the experimental setup, presented in Sect. 3.1, the wheel arch liner is prepared with a small through-hole for the connections. Additionally, the sensor system is connected to a laptop placed inside the test vehicle.

The test vehicle is a Mercedes-Benz E-Class Coupé with rear-wheel drive and summer tires with a width of 235 mm. The tire tread is asymmetric and has a depth of approximately 5 mm. Measurement data are synchronized with video material captured during test drives from outside and also with an action camera mounted on the vehicle body with view on the wheel arch liner. Test drives are performed on a brick paved road with two test routes and on a sunny day at around 22 °C.

In order to demonstrate the fundamental feasibility of our approach, two parameters are varied within the investiga-

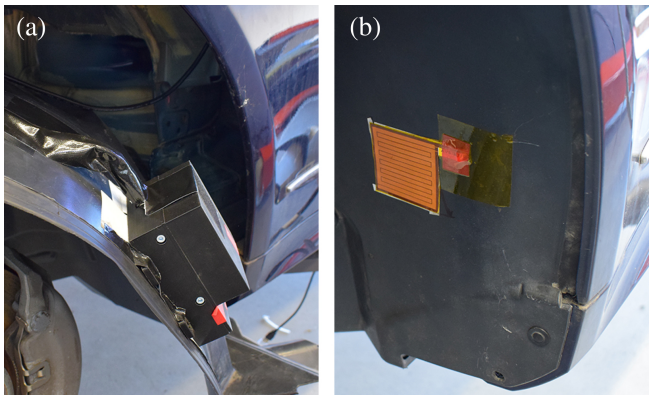

Figure 9. Integration of the sensor system into a test vehicle. **(a)** Attachment of the enclosure on the backside of the front left wheel arch liner. **(b)** Placement of the transducer on the inside of the wheel arch liner.

Table 4. Assignment of the evaluated road surface conditions and the water film height h.

Road condition	Water film height
Dry	$0\,\text{mm} \leq h < 0.01\,\text{mm}$
Damp	$0.01\,\text{mm} \leq h < 0.10\,\text{mm}$
Wet	$0.10\,\text{mm} \leq h < 0.40\,\text{mm}$
Very wet	$0.40\,\text{mm} \leq h$

tions. The first parameter is the speed, to examine whether the detection of road wetness is correlated to the speed. The other parameter to be varied is the road surface condition. For the test drives, a distinction is made between four realistic road surface conditions, which are determined by means of a commercially available reference sensor (Lufft, MARWIS). The reference sensor, which is mainly used as decision support for winter services and airports, measures the water film height h on the road surface with a non-invasive optical spectroscopy in a range from 0 to 6 mm, a resolution of 0.1 µm and a precision of ±10 % (G. Lufft Mess- und Regeltechnik GmbH, 2017). Since the reference sensor already has a classification of road surface conditions (dry, damp and wet), we adopt it and extend it by the very wet condition as shown in Table 4.

On the first test route the damp and wet road surface conditions are realized by wetting a section of the route with a length of approximately 10 m. Due to the weather and the brick road surface, the damp condition is particularly difficult to realize for exactly 10 m, whereby deviations for the test route length are possible. On this route, test drives are performed at 20 and 40 km h^{-1} with cruise control, which allows first conclusions to be drawn about the feasibility of our approach with the presented system and the influence of speed.

Figure 10. Water whirled up by the wheels during a test drive through a wetted section.

Table 5. Field test results for significant parameters of test drives on the first test route and for two speeds.

	20 km h^{-1}		40 km h^{-1}	
	ΔC_1	ΔC_2	ΔC_1	ΔC_2
Dry	1.07 pF	0.60 pF	0.56 pF	0.57 pF
Damp	12.21 pF	2.14 pF	20.66 pF	8.06 pF
Wet	179.15 pF	10.06 pF	195.90 pF	6.69 pF

The very wet road surface condition is studied on a second test route, where it is possible to have two wetted sections of a length of around 11.5 m with a dry section of approximately 70 m in between. Thus, the influence of a recurring wetting of the road surface and the behavior of the capacitance in between can be investigated. For safety reasons it is only possible to perform the test drives at 20, not at 40 km h^{-1}. Figure 10 shows a snapshot of a test drive through a wetted section. As can be seen, the water is whirled up by the wheels, which is filmed by the action camera mounted on the vehicle body.

4.3 Results

The results of capacitance against time for the first test route are presented in Fig. 11 for 20 km h^{-1} and in Fig. 12 for 40 km h^{-1}. Additionally, Table 5 summarizes two significant parameters for the first test route. While ΔC_1 represents the difference in capacitance between the dry transducer and the maximum value in the wetted section, ΔC_2 represents the difference between the dry transducer and the measurement's end after 20 s, which is not included in Figs. 11 and 12.

Since there are no water drops impinging on the transducer for a dry test road, as can be seen in Fig. 13a, ΔC_1 and ΔC_2 have the smallest values in this case for both speeds. Occurring deviations are referable to the measurement system as stated in Sect. 4.1. For the damp test road, ΔC_1 is small, with around 12 pF at 20 km h^{-1} and 21 pF at 40 km h^{-1}, since

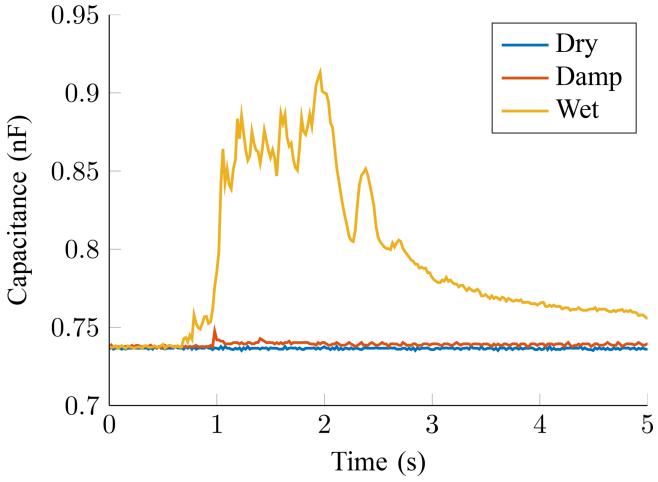

Figure 11. Field test results of capacitance against time for three different road surface conditions at 20 km h^{-1}.

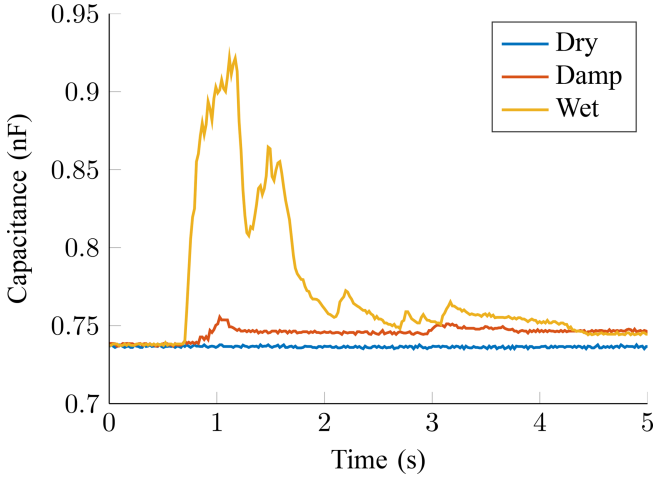

Figure 12. Field test results of capacitance against time for three different road surface conditions at 40 km h^{-1}.

the quantity of water drops impinging upon the transducer is low. Nevertheless, a distinction to the dry test road is recognizable for both speeds with the presented sensor system. In contrast, ΔC_1 for the wet test road is significantly higher in both cases, with around 179 pF at 20 km h^{-1} and 196 pF at 40 km h^{-1}, since more water drops are impinging on the transducer. Figure 13b shows a snapshot of the transducer captured during a test drive for this road condition. As can be seen, there are numerous drops impinging on the transducer and thereby causing a high capacitance.

Similar to studies at a test bench, presented in Sect. 3, water drops remain on the transducer after the end of the wet section, as shown in Fig. 13c. This causes the capacitance to fall on a plateau slightly higher than the one of a dry transducer. In contrast to the experimental results from Sect. 3.2, ΔC_2 is generally closer to zero. Besides a shorter time of drops impinging on the transducer, effects like airflow and vibrations caused by the road surface lead to more drops leaving the transducer.

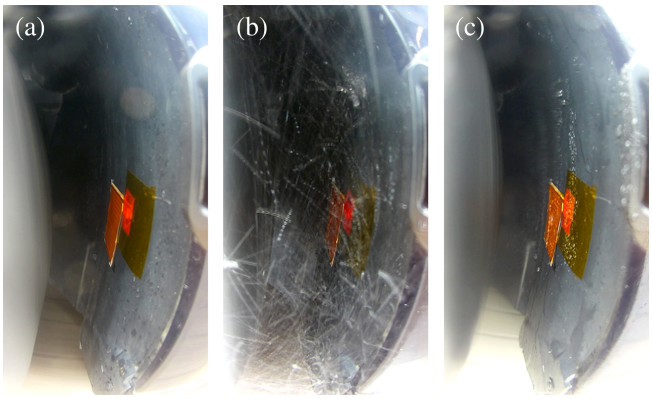

Figure 13. Snapshot of the transducer during a test drive, taken with an action camera mounted on the vehicle body for a wet test road **(a)** before, **(b)** during and **(c)** after the wet section.

The analysis of supplementary video material can help explain some effects seen in Figs. 11 and 12. After approximately 1.9 s at 20 km h^{-1} and 1.2 s at 40 km h^{-1}, the capacitance for the wet road surface condition dives for a short moment and rises again until it finally decreases to a level near the final plateau. Due to inhomogeneity on the test route, no water is whirled up for a moment, which causes the dive, as the video material shows. This indicates the potential of detecting dynamic changes in the water level thickness on a road with the proposed sensor system. After falling, there are some minor peaks at both speeds. These are caused by single water drops running down the wheel arch liner, which are recognized by the sensor system. In the case of the test drive at 40 km h^{-1}, a larger quantity of water drops runs over the transducer, causing remaining drops to follow. In addition to effects such as greater airflow and vibrations at higher speeds, this could explain the lower value of ΔC_2.

The capacitance for the damp road surface condition shows a similar behavior for 40 km h^{-1} at around 1.2 s by falling due to inhomogeneity on the test route. In contrast to the wet road surface, the capacitance does not directly rise again, since the surface is drier in this area, as the video material reveals. The peak which is recognized by the sensor system at around 3 s is caused by single water drops running down the wheel arch liner. The video material shows that the quantity of whirled-up water on the damp test route at 40 km h^{-1} is significantly higher than at 20 km h^{-1}. This explains why the results at 20 km h^{-1} show a lower and shorter increase in capacitance, rising up to a difference of around 12 pF and directly dropping down to a value only slightly higher than that of the dry transducer.

The results for the first test route reveal an influence of the speed on the quantity of whirled-up water and thereby on the measured capacitance. While the increase in capacitance for the damp road condition at 20 km h^{-1} is the lowest of

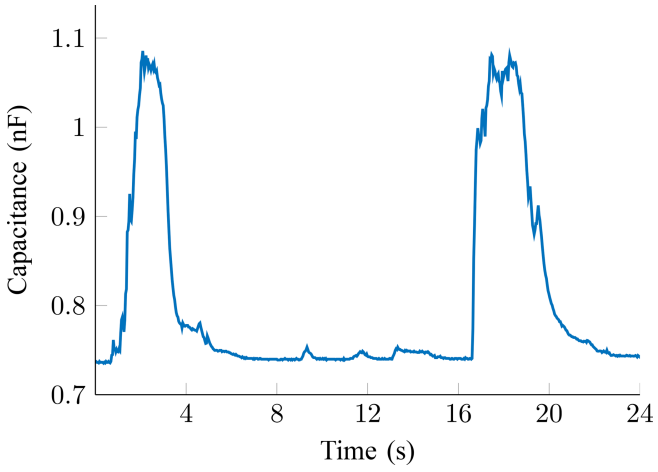

Figure 14. Field test results of capacitance against time for the very wet road surface condition.

Table 6. Field test results for significant parameters of test drives on the second test route and for the very wet road surface condition.

	ΔC_1	ΔC_2
Sector 1	352.83 pF	4.19 pF
Sector 2	353.93 pF	5.88 pF

the investigated cases with a maximum difference of around 12 pF, the capacitance increases with the speed and the water film height to a maximum difference of approximately 196 pF at 40 km h^{-1}. For both the damp and the wet road surface conditions, the increase in capacitance is larger at the higher speed. Since the differences in capacitance from road damp and wet conditions are large, even among the evaluated speeds, a distinction is possible.

In Fig. 14, the results of capacitance against time are shown for the very wet road surface condition. Due to two wetted sections on this test route, there are two major peaks for the capacitance. Since the wetting of two sections of identical size on a brick paved road is not trivial, the peaks' lengths are comparable but not equivalent. As for the first test route, ΔC_1 is used to describe the difference in capacitance between the dry transducer and the maximum value in a wetted sector. As shown in Table 6, ΔC_1 is similar for both sections, which indicates similar water layer thicknesses detected by the sensor system. Furthermore, a significant difference can be seen between the wet (Table 5) and very wet (Table 6) road surface conditions, even among the evaluated speeds. Therefore, a distinction between the investigated road surface conditions is possible with the presented approach.

Considering ΔC_2, which describes the difference between the dry transducer and the measurement's end of each section, the results of the first test route can be confirmed. Immediately after the wetted route is passed, the capacitance falls down to a value slightly higher than of a dry transducer. Since there is a greater period without new water whirled up after the first peak, ΔC_2 of Sector 1 is lower due to effects like airflow and vibrations caused by the road surface. The minor peaks, for example at around 9 and 13 s, are caused by single water drops running down the wheel arch liner as the video material shows.

5 Conclusions

This work presented a novel approach for detecting road surface wetness with planar capacitive sensors on the wheel arch liner of a motor vehicle. In the first part of the work we investigated the effect of various design parameters for planar interdigital electrodes by three-dimensional electrostatic FEM simulations considering the detection of water. The results demonstrate a trade-off between penetration depth and the dynamic range or measurement sensitivity and propose a suitable design for the detection of whirled-up water. A transducer was manufactured as a flexible PCB and was investigated by means of an experimental study on a motor vehicle's front wheel arch liner by simulating realistic road surface scenarios on a test bench. The quantity and size of the water drops used to simulate the whirled-up water show a correlation to the capacitance which allows the distinction between different scenarios. Furthermore, it is possible to detect a static wetting of the wheel arch liner.

In order to study our approach in the field, a sensor system for measurements in the vehicle was presented. In experiments at a test bench, the sensor system showed a similar behavior as a reference measuring instrument for different wetness levels. Although the standard deviation was higher for the sensor system, it was suitable for practical tests and thereby integrated into a vehicle. Field test results demonstrate the feasibility to differentiate between wetness levels on two test routes. Furthermore, the results show a correlation of the speed and the quantity of whirled-up water. Even though the increase in capacitance is low for a damp road surface, especially for lower speed, a distinction between wetness levels is still possible for the evaluated speeds and road conditions. Thereby, the potential of detecting road surface wetness with planar capacitive sensors on the wheel arch liner of a motor vehicle is demonstrated.

The presented approach can prospectively contribute to increase the safety of passengers and traffic participants in times of highly or fully automated driving. Different issues have to be investigated in future work, such as the influence of tire characteristics on the quantity and size of whirled-up water drops and thereby on the detected capacitance. In addition, further studies will be carried out with regard to the influence of higher speeds, since the critical-safety relevance of road surface wetness increases with speed. Moreover, the transducer and its positioning in the wheel arch liner will be further optimized. In consequence, an array of transducers

is also conceivable, as different positions might provide additional information with respect to speed and road surface wetness dependency.

Data availability. The underlying measurement data are not publicly available and can be requested from the authors, if required.

Author contributions. KLK supervised the project and proofread the paper. JD performed the simulations. JH prepared the planar capacitive transducer. JD and LT carried out the experiments. JD developed the sensor system and carried out the field test. JD prepared the paper.

Competing interests. The authors declare that they have no conflict of interest.

Special issue statement. This article is part of the special issue "Sensors and Measurement Systems 2018". It is a result of the "Sensoren und Messsysteme 2018, 19. ITG-/GMA-Fachtagung", Nürnberg, Germany, from 26 June 2018 to 27 June 2018.

Acknowledgements. This work is funded by the German Federal Ministry for Economic Affairs and Energy, project SEEROAD.

Edited by: Stefan Rupitsch
Reviewed by: two anonymous referees

References

Baxter, L. K.: Capacitive Sensors: Design and Applications, Wiley-IEEE Press, New York, https://doi.org/10.1109/9780470544228, 1997.

Brasseur, G.: Design rules for robust capacitive sensors, IEEE T. Instrum. Meas., 52, 1261–1265, https://doi.org/10.1109/TIM.2003.816812, 2003.

Canbolat, H.: A Novel Level Measurement Technique Using Three Capacitive Sensors for Liquids, IEEE T. Instrum. Meas., 58, 3762–3768, https://doi.org/10.1109/TIM.2009.2019715, 2009.

Chen, Z. and Luo, R. C.: Design and implementation of capacitive proximity sensor using microelectromechanical systems technology, IEEE T. Ind. Electron., 45, 886–894, https://doi.org/10.1109/41.735332, 1998.

Da Silva, M.: Impedance sensors for fast multiphase flow measurement and imaging, Ph.D. dissertation, Technical University of Dresden, 2008.

Dean, R. N., Rane, A. K., Baginski, M. E., Richard, J., Hartzog, Z., and Elton, D. J.: A Capacitive Fringing Field Sensor Design for Moisture Measurement Based on Printed Circuit Board Technology, IEEE T. Instrum. Meas., 61, 1105–1112, https://doi.org/10.1109/TIM.2011.2173041, 2012.

G. Lufft Mess- und Regeltechnik GmbH: Operating Manual MARWIS-UMB/STARWIS-UMB, 2017.

Happel, J., Döring, J., Krieger, K.-L., Deitschun, J., and Godlinski, D.: Printed Capacitive Sensors for Contactless Ice Detection in Automotive Liquid Conveyor Pipes, in: AMA Conferences – Proceedings Sensor, 621–626, https://doi.org/10.5162/sensor2017/P3.2, 2017.

Hu, X. and Yang, W.: Planar capacitive sensors – designs and applications, Sensor Rev., 30, 24–39, https://doi.org/10.1108/02602281011010772, 2010.

Karuthedath, C. B. and George, B.: A capacitive ice layer detection system suitable for autonomous inspection of runways using an ROV, in: 2012 IEEE International Symposium on Robotic and Sensors Environments Proceedings, 16–18 November, Magdeburg, 127–132, https://doi.org/10.1109/ROSE.2012.6402627, 2012.

Li, X. B., Larson, S. D., Zyuzin, A. S., and Mamishev, A. V.: Design of multichannel fringing electric field sensors for imaging, Part I, General design principles, in: Conference Record of the 2004 IEEE International Symposium on Electrical Insulation, 19–22 September, Indianapolis, 406–409, https://doi.org/10.1109/ELINSL.2004.1380616, 2004.

Li, X. B., Larson, S. D., Zyuzin, A. S., and Mamishev, A. V.: Design principles for multichannel fringing electric field sensors, IEEE Sens. J., 6, 434–440, https://doi.org/10.1109/JSEN.2006.870161, 2006.

Mamishev, A. V., Sundara-Rajan, K., Yang, F., Du, Y., and Zahn, M.: Interdigital sensors and transducers, Proc. IEEE, 92, 808–845, https://doi.org/10.1109/JPROC.2004.826603, 2004.

Mizuguchi, J., Piai, J. C., de França, J. A., de Morais França, M. B., Yamashita, K., and Mathias, L. C.: Fringing Field Capacitive Sensor for Measuring Soil Water Content: Design, Manufacture, and Testing, IEEE T. Instrum. Meas., 64, 212–220, https://doi.org/10.1109/TIM.2014.2335911, 2015.

Texas Instruments: FDC2x1x EMI-Resistant 28-Bit,12-Bit Capacitance-to-Digital Converter for Proximity and Level Sensing Applications, 2015.

Troiano, A., Pasero, E., and Mesin, L.: An innovative water and ice detection system for monitoring road and runway surfaces, in: 6th Conference on Ph.D. Research in Microelectronics Electronics, 18–21 July, Berlin, 1–4, 2010.